Cavity-QED Quantum Simulator of Dynamical Phases of a Bardeen-Cooper-Schrieffer Superconductor

Robert J. Lewis-Swan,[1,2,3,4] Diego Barberena,[3,4] Julia R. K. Cline,[3] Dylan J. Young,[3] James K. Thompson,[3] and Ana Maria Rey[3,4]

[1]Homer L. Dodge Department of Physics and Astronomy, The University of Oklahoma, Norman, Oklahoma 73019, USA
[2]Center for Quantum Research and Technology, The University of Oklahoma, Norman, Oklahoma 73019, USA
[3]JILA, NIST, Department of Physics, University of Colorado, Boulder, Colorado 80309, USA
[4]Center for Theory of Quantum Matter, University of Colorado, Boulder, Colorado 80309, USA

(Received 2 December 2020; accepted 22 March 2021; published 27 April 2021)

We propose to simulate dynamical phases of a BCS superconductor using an ensemble of cold atoms trapped in an optical cavity. Effective Cooper pairs are encoded via the internal states of the atoms, and attractive interactions are realized via the exchange of virtual photons between atoms coupled to a common cavity mode. Control of the interaction strength combined with a tunable dispersion relation of the effective Cooper pairs allows exploration of the full dynamical phase diagram of the BCS model as a function of system parameters and the prepared initial state. Our proposal paves the way for the study of the nonequilibrium features of quantum magnetism and superconductivity by harnessing atom-light interactions in cold atomic gases.

DOI: 10.1103/PhysRevLett.126.173601

Introduction.—The development of a generic framework to understand the properties of nonequilibrium quantum states is a long-standing challenge in modern physics. Theoretical work [1–6] combined with technical advances in the control and characterization of many-body physics in cold atom experiments [7–15] has led to new developments in this direction, such as extending the concept of phase transitions to nonequilibrium situations. Specifically, dynamical phase transitions [1,16–20] have been introduced to classify distinct regimes of dynamical behavior that arise after a sudden quench of a control parameter in a closed system. Dynamical phase transitions are characterized by the existence of a time-averaged order parameter that demonstrates nonanalytic behavior at the boundary between dynamical phases.

A long-standing example of such dynamical phases are those predicted to emerge from quenches of BCS superconductors, which have been theoretically investigated in both the condensed matter [21–30] and high energy communities [31]. However, experimental progress toward observing these phases has been limited so far to transient dynamics on rapid timescales in terahertz pump-probe experiments [32,33]. Recent proposals to enhance pairing by coupling materials to cavities and adjustable external laser driving might facilitate probing the predicted BCS phases in solid state systems [34].

Here, motivated by developments studying dynamical phase transitions in state-of-the-art quantum simulators, we present a proposal to emulate the nonequilibrium dynamics of the BCS model of superconductivity with cavity-QED [9,13,35–38]. Our scheme leverages the tunability and control available in this platform to map out the dynamical phase diagram over a broad range of system parameters and initial states, demonstrating the power of cavity-QED systems as quantum simulators of superconductivity and quantum magnetism [39–42].

BCS model and dynamical phases.—The BCS model of superconductivity for s-wave interacting fermions is characterized by the Hamiltonian [43]

$$\hat{H} = -\chi \sum_{\mathbf{k},\mathbf{k}'} \hat{c}^{\dagger}_{\mathbf{k},\uparrow} \hat{c}^{\dagger}_{-\mathbf{k},\downarrow} \hat{c}_{\mathbf{k}',\uparrow} \hat{c}_{-\mathbf{k}',\downarrow} + \sum_{\mathbf{k},\sigma} \varepsilon_{\mathbf{k}} \hat{c}^{\dagger}_{\mathbf{k},\sigma} \hat{c}_{\mathbf{k},\sigma}. \quad (1)$$

Here, $\hat{c}^{\dagger}_{\mathbf{k},\sigma}$ ($\hat{c}_{\mathbf{k},\sigma}$) creates (annihilates) a fermion of momentum $\mathbf{k}$ and spin $\sigma = \uparrow, \downarrow$. The first term describes attractive s-wave interactions $\chi \geq 0$ that lead to the formation of Cooper pairs. The single-particle dispersion is $\varepsilon_{\mathbf{k}} = \mathbf{k}^2/(2m) - \mu$ with μ the chemical potential and m the particle mass. Throughout the manuscript, we set $\hbar = 1$.

This "reduced" BCS model assumes that only Cooper pairs are created and destroyed with zero center-of-mass momentum and neglects pair-breaking processes, so the low-energy physics can be described using only the presence or absence of Cooper pairs at each momentum mode. The physics of the model is further simplified by introducing the Anderson pseudospin-1/2 operators

$$\hat{\sigma}^{-}_{\mathbf{k}} = \hat{c}_{\mathbf{k},\uparrow} \hat{c}_{-\mathbf{k},\downarrow}, \quad \hat{\sigma}^{z}_{\mathbf{k}} = \hat{c}^{\dagger}_{\mathbf{k},\uparrow} \hat{c}_{\mathbf{k},\uparrow} + \hat{c}^{\dagger}_{-\mathbf{k},\downarrow} \hat{c}_{-\mathbf{k},\downarrow} - 1. \quad (2)$$

The two eigenstates of $\hat{\sigma}^z_{\mathbf{k}}$ encode the presence or absence of a Cooper pair with momentum $\mathbf{k}$, which are created (annihilated) by $\hat{\sigma}^+_{\mathbf{k}}$ ($\hat{\sigma}^-_{\mathbf{k}}$). Equation (1) then becomes

$$\hat{H} = -\chi \sum_{\mathbf{k},\mathbf{k}'} \hat{\sigma}^+_{\mathbf{k}} \hat{\sigma}^-_{\mathbf{k}'} + \sum_{\mathbf{k}} \varepsilon_{\mathbf{k}} \hat{\sigma}^z_{\mathbf{k}} = -\chi \hat{S}^+ \hat{S}^- + \sum_{\mathbf{k}} \varepsilon_{\mathbf{k}} \hat{\sigma}^z_{\mathbf{k}}, \tag{3}$$

where $\hat{S}^{\pm} = \sum_{\mathbf{k}} \hat{\sigma}^{\pm}_{\mathbf{k}}$ are collective spin operators.

The ground state $|\psi\rangle_{\mathrm{gs}}$ of Eq. (3) within BCS theory is characterized by the expectations [26]

$$\langle \hat{\sigma}^+_{\mathbf{k}} \rangle_{\mathrm{gs}} = \frac{1}{2} \frac{\Delta_{\mathrm{gs}}}{\sqrt{\Delta^2_{\mathrm{gs}} + \varepsilon^2_{\mathbf{k}}}}, \qquad \langle \hat{\sigma}^z_{\mathbf{k}} \rangle_{\mathrm{gs}} = \frac{\varepsilon_{\mathbf{k}}}{\sqrt{\Delta^2_{\mathrm{gs}} + \varepsilon^2_{\mathbf{k}}}}, \tag{4}$$

as shown schematically on the Bloch sphere in Fig. 1(b). Here, the BCS pairing gap $\Delta_{\mathrm{gs}} \equiv \chi \langle \hat{S}^- \rangle_{\mathrm{gs}}$ is defined self-consistently.

Prior studies in superconductors and fermionic superfluids [26,27,44] have used the BCS Hamiltonian, Eq. (3), to describe the gap dynamics after a quench of the pairing gap from the ground-state value Δ_{gs} to a final value Δ_f [26,27]. Equation (3) is expected to provide a valid treatment of the gap dynamics on timescales for which pair-breaking processes can be neglected, provided the quench is done faster than the inverse of the quasiparticle gap.

In the mean-field (classical) limit, the dynamics falls into three distinct dynamical phases according to the behavior of the magnitude of $|\Delta(t)| = \chi |S^-(t)|$. Throughout, we adopt the notation $\mathcal{O}(t) \equiv \langle \hat{\mathcal{O}}(t) \rangle$ when making a mean-field approximation, i.e., $\langle \hat{\mathcal{O}}_1(t) \hat{\mathcal{O}}_2(t) \rangle = \langle \hat{\mathcal{O}}_1(t) \rangle \langle \hat{\mathcal{O}}_2(t) \rangle$. As $t \to \infty$, the dynamics are Phase I, $|\Delta(t)| \to 0$; Phase II, $|\Delta(t)| \to$ const with transient oscillations that decay as $\propto t^{-1/2}$; or Phase III, $|\Delta(t)|$, which features persistent oscillations. Illustrations of $|\Delta(t)|$ in each phase are shown in Fig. 1(a). We discuss below how these phases arise from a competition between the interactions and the distribution of single-particle splittings $\varepsilon_{\mathbf{k}}$.

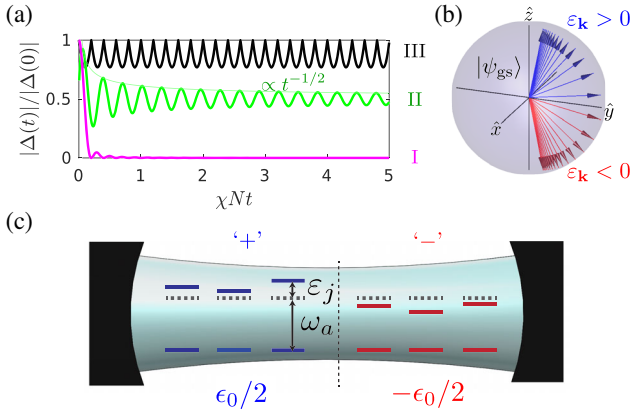

FIG. 1. (a) BCS dynamical phases illustrated by the pairing amplitude $|\Delta(t)|$. Characteristic $t^{-1/2}$ decay of Phase II is indicated by the faded line. (b) Example BCS ground state on the Bloch sphere. The single-particle inversion $\langle \hat{\sigma}^z_{\mathbf{k}} \rangle$ correlates with the sign of the dispersion $\varepsilon_{\mathbf{k}}$ [Eq. (4)]. (c) BCS physics can be simulated in a cavity by encoding a spin-1/2 into a pair of internal atomic states with transition frequency ω_a, which are coupled to a single common cavity mode. The spin-1/2 atoms are divided into two ensembles (shown as blue and red) featuring mean energy splittings with opposite sign, $\pm\epsilon_0/2$.

BCS physics in a cavity-QED simulator.—We propose to explore the phase diagram of the BCS model by emulating the Hamiltonian, Eq. (3), in a cavity. In our proposed scheme, an ensemble of atoms is distributed in a standing wave optical lattice supported by the cavity. Each atom, which we index by the label j, encodes a spin-1/2 degree of freedom in a pair of stable internal states, $|\uparrow\rangle_j$ and $|\downarrow\rangle_j$, which map to the presence or absence of a Cooper pair, respectively. The use of the index j compared to the momentum label $\mathbf{k}$ in a real BCS superconductor will be shown to be irrelevant.

Spin-spin interactions $\propto \hat{S}^+ \hat{S}^-$ are mediated by the exchange of virtual photons between atoms via a single common cavity mode (at frequency ω_c) far-detuned from the atomic resonance (at frequency ω_a) [9,35,45,46]. These photon-mediated interactions are analogous to the phonon-mediated interactions in a BCS superconductor. Tunable (inhomogeneous) single-particle energy shifts $\varepsilon_j \hat{\sigma}^z_j$ can be realized via external fields that generate time-varying AC Stark or Zeeman shifts of the internal atomic states.

An important ingredient for the observation of the dynamical Phases I–III is the ability to prepare initial states correlated with the distribution of splittings ε_j. For example, in the BCS ground state [Eq. (4)], the sign of the inversion $\langle \hat{\sigma}^z_{\mathbf{k}} \rangle$ of the Anderson pseudospins correlates with the sign of the single-particle dispersion $\varepsilon_{\mathbf{k}}$. Motivated by this case, we consider initial states where the atoms are split into a pair of ensembles where the spin configuration of the atoms in each ensemble is correlated with the sign of the ensemble's average splitting. Concretely, we consider $2N$ atoms divided into two equal ensembles and initialized as a product of coherent spin states [47] lying on the equatorial plane of the Bloch sphere separated by a relative azimuthal opening angle $\Delta\phi_0$: $|\psi_0\rangle = |\pi/2, \Delta\phi_0/2\rangle_+ \otimes |\pi/2, -\Delta\phi_0/2\rangle_-$ [see Fig. 1 and Fig. 2(a)] where the subscript $\pm$ denotes each ensemble. Here, $|\theta, \phi\rangle \equiv \bigotimes_j [\cos(\theta/2)|\downarrow\rangle_j + e^{i\phi} \sin(\theta/2)|\uparrow\rangle_j]$ where the product runs over $j = 1, \ldots, N$ or $j = N+1, \ldots, 2N$ atoms, respectively, for the $\pm$ ensembles. Lastly, following the BCS ground state, we assume a uniform distribution of splittings $\varepsilon_j \in [\pm\epsilon_0/2 - W/4, \pm\epsilon_0/2 + W/4]$, where the sign of ϵ_0 differs for each ensemble and is matched to the sign of $\pm\Delta\phi_0/2$. It is the mean $\pm\epsilon_0/2$ and characteristic width $W/2$ rather than the precise distribution of ε_j (e.g., uniform

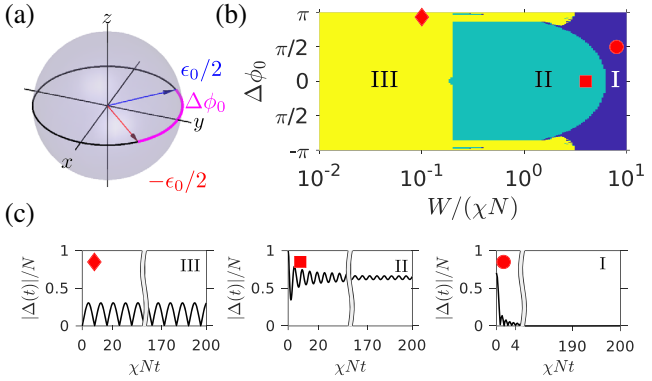

FIG. 2. (a) Typical initial state for opening angle $\Delta\phi_0$. The orientation of each ensemble (red and blue collective Bloch vectors) is correlated with the sign of $\pm\epsilon_0$. (b) Mean-field BCS dynamical phase diagram as a function of $\Delta\phi_0$ and characteristic width W of the single-particle noise distribution, with fixed $\epsilon_0/(\chi N) = 0.1$. The phase diagram is evaluated numerically (see Ref. [48]), and some small structures (e.g., regions of Phase II within Phase III) are likely artifacts of the method's precision. (c) Time traces of the pairing amplitude $|\Delta(t)|$ for each phase [parameters indicated by marker in (b)].

or normal) that are important to characterizing the physics discussed below.

Preparation of the two ensembles and correlation with $\pm\epsilon_0$ can be achieved by spatially selective energy shifts of atoms in the cavity [45] [Fig. 1(c)] or by addressing different internal levels [35,51] (see later discussion) [52].

Accessible dynamical phase diagram.—In Fig. 2, we explore the accessible dynamical phases. Panel (b) shows the dynamical phase diagram for mean splitting $\epsilon_0/(\chi N) = 0.1$. The phase diagram is computed via a Lax analysis [24,26,27], which is a method for integrable models such as Eq. (3) to determine the frequency spectrum that rules the dynamics of the order parameter. The spectrum is extracted from the roots of $L^2(u)$, the squared norm of the Lax vector $\mathbf{L}(u)$, a polynomial defined in terms of a complex variable u that encodes the conserved quantities of the model. A spectrum with all real roots defines Phase I, with one pair of complex roots Phase II and with two pairs of complex roots Phase III. The asymptotic behavior of $|\Delta(t)|$ follows from the nature of the roots of $L^2(u)$, which we compute numerically [48].

Physically, the dynamical phases depend on the competition between single-particle dephasing generated by W and ϵ_0 and the spin-locking effect generated by the interactions with strength set by χN [53–60]. The spin locking is induced by the existence of a many-body gap that suppresses local spin flips and favors spin alignment [35,36,61]. Such behavior also resembles the synchronization observed in arrays of coupled oscillators with dissipation [62,63]. Other consequences associated with the many-body gap include the stabilization of localization effects in fully connected models under specific initial conditions [64,65].

For the small inhomogeneity $W \ll \epsilon_0, \chi N$, we predict Phase III dynamics independent of the opening angle $\Delta\phi_0$. Within each ensemble, a gap opens between the manifold of collective states (this includes the initial fully polarized states) and those that are spatially inhomogeneous, preventing dephasing of the individual spins of each ensemble. In addition, the interplay between the homogeneous single-particle energy splitting $\pm\epsilon_0$ (that generates precession of the ensembles in opposing directions about the z axis of the Bloch sphere), and the collective interaction (that also drives a rotation of each ensemble along a common self-generated axis set by the total transverse magnetization [35,51]), leads to persistent nonlinear oscillations in the effective pairing amplitude $|\Delta(t)| = |S^+(t)|$ [see also Fig. 3(a)].

Phase II emerges for $2\epsilon_0 < W \lesssim \chi N$ and opening angles away from $\Delta\phi \approx \pm\pi$ [48]. The transition from Phase III to II is driven by the ensembles no longer having a well-defined relative energy splitting correlated with their initial orientation. Thus, in contrast to Phase III, spin locking of the *entire* ensemble of $2N$ atoms determines the dynamics. This means that, while the pairing amplitude $|\Delta(t)|$ remains large, oscillations are transient and suppressed rather than stabilized by the interactions.

Finally, Phase I emerges for $W \gtrsim \chi N$ independent of ϵ_0. Single-particle physics dominates for all initial conditions, and the pairing amplitude vanishes due to rapid dephasing of the individual spins, $|\Delta(t)| \to 0$.

Beyond these three known regimes, we also predict the emergence of two previously unidentified subphases within Phase III for $W \ll \chi N$, ϵ_0, which we label as IIIa and IIIb.

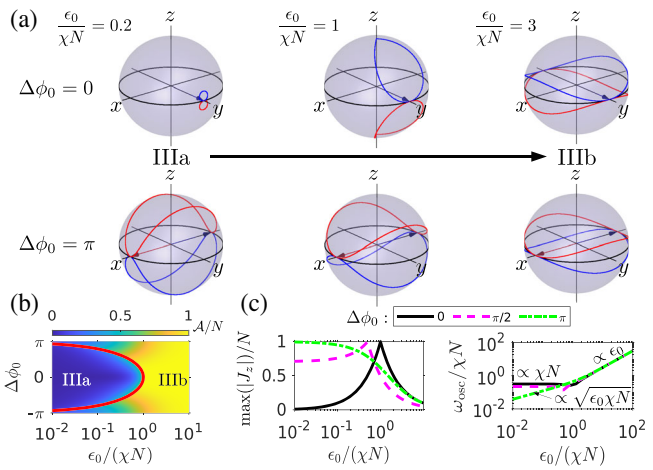

FIG. 3. (a) Typical trajectories of the collective Bloch vector of each ensemble (red and blue) for $W \ll \chi N$, ϵ_0 as ϵ_0 is tuned between Phases IIIa and IIIb. (b) Phase diagram characterized by amplitude $\mathcal{A} \equiv \max(|\Delta(t)|) - \min(|\Delta(t)|)$ of oscillations in $|\Delta(t)|$. The critical boundary ϵ_0^c between Phases IIIa and IIIb is indicated by the red line. (c) Maximum of the total inversion difference $J_z = (\sum_{j\in+}\sigma_j^z - \sum_{j\in-}\sigma_j^z)/2$ and frequency $\omega_{\rm osc}$ of oscillations of $|\Delta(t)|$ as a function of ϵ_0.

These subphases are delineated by a critical splitting $\epsilon_0^c = (\chi N/2)[1+\cos(\Delta\phi_0)]$ [48]. Phase IIIa, $\epsilon_0 < \epsilon_0^c$, is dominated by interactions and characterized by a strictly nonzero pairing amplitude, $|\Delta(t)| > 0$, that exhibits nonlinear oscillations with an approximate frequency $\omega_{\rm osc} \propto \chi N$. Phase IIIb is characterized by the pairing amplitude periodically vanishing, $|\Delta(t)| = 0$, and the physics is dominated by the single-particle splitting ϵ_0 such that the frequency of oscillations scales as $\omega_{\rm osc} \propto \epsilon_0$.

In Fig. 3(a), we illustrate typical trajectories of the collective Bloch vector of each ensemble in subphases IIIa and IIIb for an initial state with $\Delta\phi_0 = 0$, which are representative of the dominant physics for $|\Delta\phi_0| \lesssim \pi$. For small $\epsilon_0 \ll \epsilon_0^c$ and $\Delta\phi_0 \ll \pi$, the Bloch vectors remain trapped close to their initial polarization due to the strong interactions, leading to $|\Delta(t)| > 0$. As ϵ_0 increases nearer to the transition ϵ_0^c, the interactions still dominate and their interplay with the single-particle term leads to a deflection of the trajectories of the Bloch vectors close to the north and south poles. Above ϵ_0^c, the trajectories abruptly snap to large orbits near the equator and quickly approach the precession expected for two independent ensembles (e.g., dominated by the $\hat{\sigma}_z$ term of the Hamiltonian). Even though Phase IIIb is technically absent for $\Delta\phi_0 = \pm\pi$ by our definition (as $|\Delta(0)| = 0$), we still observe rich nontrivial oscillations for $\epsilon_0 \ll \chi N$ with frequency $\omega_{\rm osc} \propto \sqrt{\epsilon_0 \chi N}$ [48].

Quantitatively, the IIIa and IIIb subphases are delineated by abrupt changes in different observables, including the magnitude $\mathcal{A} \equiv \max(|\Delta(t)|) - \min(|\Delta(t)|)$, the frequency $\omega_{\rm osc}$ of oscillations of $|\Delta(t)|$ [Figs. 3(b) and 3(d)] and the maximum excursion of the collective spins away from the equator of the Bloch sphere, measured by the differential inversion $J_z = (\sum_{j\in+}\sigma_j^z - \sum_{j\in-}\sigma_j^z)/2$ [Fig. 3(c)].

Experimental realization and robustness of proposal.—In a cavity-QED experiment, the dynamical phases can be characterized by detection of intracavity light leaking out through the cavity mirrors [35]. By operating in the limit where the cavity mode is far off-resonance from the atomic transition, the virtual photons that mediate the interactions are adiabatically eliminated and slaved to the spins, such that atomic information is imprinted onto the phase and amplitude of the cavity field via the approximate relation $a(t) \propto S^-(t) \propto \Delta(t)$ [35,48]. The light intensity then serves as a proxy for the BCS pairing amplitude, $|a(t)|^2 \propto |\Delta(t)|^2$, while the frequency spectrum of $a(t)$ can also be a useful diagnostic to distinguish the dynamical phases. Moreover, by continuously performing heterodyne detection of the small amount of light leaking through the cavity mirrors, we are able, in principle, to construct time traces of the pairing amplitude within a single experimental trial.

To demonstrate that our proposal is robust to relevant decoherence and technical factors, we model an experiment where the spin-1/2 is encoded using the narrow linewidth $^1S_0$-$^3P_1$ optical transition of ^{87,88}Sr. Here, subensembles can be prepared via spatially dependent light shifts from the side of the cavity, or in ^{87}Sr by applying spatially dependent magnetic fields and addressing the $\pm 9/2$ nuclear spin levels of the transition. We use parameters from Ref. [9] and include single-particle decoherence due to the natural linewidth of the transition $\gamma/(2\pi) = 7.5$ kHz and spatially inhomogeneous atom-light coupling arising due to the incommensurate wavelengths of the standing wave optical lattice confining the atoms and the relevant cavity mode [9,35,48]. The latter leads to a spatial modulation of the spin-spin interactions $\chi \to \chi_{i,j}$. Our predictions should also be qualitatively relevant for other cavity-based systems that can realize an effective $\chi\hat{S}^+\hat{S}^-$ interaction, e.g., Raman transitions [45,46].

In Fig. 4(a), we model the transition between Phases I and III as a function of the inhomogeneity strength W at fixed $\epsilon_0/(\chi N) = 0.1$ and initial state $\Delta\phi_0 = \pi$. The phases are distinguished in the frequency spectrum of the cavity

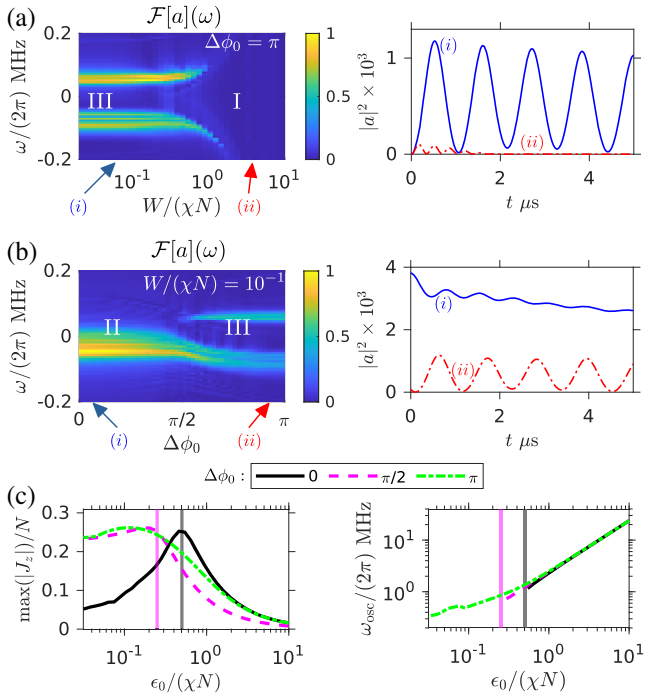

FIG. 4. Dynamics of intracavity field $a(t)$. (a) Frequency spectrum of intracavity field $\mathcal{F}[a](\omega)$ as a function of $W/(\chi N)$, and typical time traces of $|a|^2$ in Phases (i) III and (ii) I. Initial state is $\Delta\phi_0 = \pi/2$. (b) Same but as a function of opening angle $\Delta\phi_0$ and time traces are in Phases (i) II and (ii) III. Simulations are for fixed $W/(\chi N) = 0.1$. Both (a) and (b) use fixed $\epsilon_0/(\chi N) = 0.1$, and color scales are normalized. (c) Signatures of Phase IIIa and Phase IIIb in differential inversion J_z and oscillation frequency $\omega_{\rm osc}$ of $|a|^2$ for $W = 0$ for different $\Delta\phi_0$. Critical ϵ_0^c for each $\Delta\phi_0$ is indicated by a vertical line. The absence of plotted results for $\omega_{\rm osc}$ below the approximate transition ϵ_0^c for each $\Delta\phi_0$ indicates the lack of appreciable oscillations in the simulations. All relevant parameters (e.g., g, γ, and κ) are taken from Refs. [9,35], and results are rescaled for $N = 10^6$ (see also Ref. [48]).

field $\mathcal{F}[a](\omega)$, with Phase III signaled by a pair of robust peaks in the spectrum that disappear in Phase I. The peaks are consistent with the entwined but distinguishable precession of the two ensembles that leads to beating of the intensity $|a(t)|^2$, as shown in the accompanying time trace. The oscillations in the intracavity intensity $|a(t)|^2$ are robust to the inhomogeneous interactions and the exponential decay induced by γ. The transition between the phases III and I occurs at $W/(\chi N) \approx \pi/2$. This is consistent with the model Eq. (3) when the inhomogeneous atom-light coupling is taken into account by a simple rescaling to the corresponding mean value $\chi \to \overline{\chi_{i,j}} = \chi/2$ [48].

Similarly, in Fig. 4(b) the Phase II–III transition can be observed by varying the initial opening angle $\Delta\phi_0$ at fixed $W/(\chi N) = \epsilon_0/(\chi N) = 0.1$. The spectrum of the intracavity field shows the signature dual peaks of Phase III for $\pi/2 \lesssim \Delta\phi_0 \leq \pi$, while Phase II is signaled by a single peak for $0 \leq \Delta\phi_0 \lesssim \pi/2$. The latter indicates dynamics of a single collective ensemble, with finite but non-oscillatory pairing amplitude.

Lastly, signatures of the Phase IIIa–IIIb transition in the differential inversion and oscillation frequency of $|a(t)|^2$ are shown in Fig. 4(c). Decoherence blunts the expected cusp in the inversion, although the peak value lines up closely with the expected transition upon accounting for inhomogeneous interactions. The oscillation frequency clearly distinguishes the trivial and nontrivial regimes for $\Delta\phi_0 = \pi$. On the other hand, we find that, for $\Delta\phi_0 = 0$, $\pi/2$, the relatively small oscillations in $|a(t)|^2$ predicted for Phase IIIa are destroyed by decoherence, and instead the transition between IIIa and IIIb is marked by an abrupt vanishing of any discernible peak in the spectrum (indicated by the absence of data).

Conclusions.—We have reported a proposal to observe the dynamical phases of a BCS superconductor in a cavity-QED quantum simulator. Realizing these phases via a spin degree of freedom instead of actual Cooper pairs overcomes the need to reach the ultracold temperatures at which pairing occurs. The versatility of this platform allows us to probe the dependence of the dynamical phases on the initial state and system parameters in a controllable, isolated setting. Our predictions pave the way for future studies of more complex non-equilibrium phenomena in models of quantum magnetism and superconductivity so far not seen in real materials or high energy systems.

We acknowledge helpful discussions with Anjun Chu, Nathan Schine, Victor Gurarie. and Emil Yuzbashyan. This work is supported by the AFOSR Grant No. FA9550-18-1-0319, by the DARPA and ARO Grant No. W911NF-16-1-0576, the ARO single investigator Grant W911NF-19-1-0210, the NSF PHY1820885, NSF JILA-PFC PHY-1734006 and NSF QLCI-2016244 grants, and by NIST, the U.S. Department of Energy, Office of Science, National Quantum Information Science Research Centers, Quantum Systems Accelerator (QSA).

[1] B. Sciolla and G. Biroli, Dynamical transitions and quantum quenches in mean-field models, J. Stat. Mech. (2011) P11003.
[2] M. Heyl, A. Polkovnikov, and S. Kehrein, Dynamical Quantum Phase Transitions in the Transverse-Field Ising Model, Phys. Rev. Lett. **110**, 135704 (2013).
[3] M. Heyl, Dynamical quantum phase transitions: A review, Rep. Prog. Phys. **81**, 054001 (2018).
[4] B. Žunkovič, M. Heyl, M. Knap, and A. Silva, Dynamical Quantum Phase Transitions in Spin Chains with Long-Range Interactions: Merging Different Concepts of Non-equilibrium Criticality, Phys. Rev. Lett. **120**, 130601 (2018).
[5] S. B. Jäger, J. Cooper, M. J. Holland, and G. Morigi, Dynamical Phase Transitions to Optomechanical Superradiance, Phys. Rev. Lett. **123**, 053601 (2019).
[6] C.-M. Halati, A. Sheikhan, H. Ritsch, and C. Kollath, Numerically Exact Treatment of Many-Body Self-Organization in a Cavity, Phys. Rev. Lett. **125**, 093604 (2020).
[7] P. Jurcevic, H. Shen, P. Hauke, C. Maier, T. Brydges, C. Hempel, B. P. Lanyon, M. Heyl, R. Blatt, and C. F. Roos, Direct Observation of Dynamical Quantum Phase Transitions in an Interacting Many-Body System, Phys. Rev. Lett. **119**, 080501 (2017).
[8] J. Zhang, G. Pagano, P. W. Hess, A. Kyprianidis, P. Becker, H. Kaplan, A. V. Gorshkov, Z.-X. Gong, and C. Monroe, Observation of a many-body dynamical phase transition with a 53-qubit quantum simulator, Nature (London) **551**, 601 (2017).
[9] J. A. Muniz, D. Barberena, R. J. Lewis-Swan, D. J. Young, J. R. K. Cline, A. M. Rey, and J. K. Thompson, Exploring dynamical phase transitions with cold atoms in an optical cavity, Nature (London) **580**, 602 (2020).
[10] S. Smale, P. He, B. A. Olsen, K. G. Jackson, H. Sharum, S. Trotzky, J. Marino, A. M. Rey, and J. H. Thywissen, Observation of a transition between dynamical phases in a quantum degenerate fermi gas, Sci. Adv. **5**, eaax1568 (2019).
[11] T. Tian, H.-X. Yang, L.-Y. Qiu, H.-Y. Liang, Y.-B. Yang, Y. Xu, and L.-M. Duan, Observation of Dynamical Quantum Phase Transitions with Correspondence in an Excited State Phase Diagram, Phys. Rev. Lett. **124**, 043001 (2020).
[12] A. Chu, J. Will, J. Arlt, C. Klempt, and A. M. Rey, Simulation of xxz Spin Models Using Sideband Transitions in Trapped Bosonic Gases, Phys. Rev. Lett. **125**, 240504 (2020).
[13] K. Baumann, C. Guerlin, F. Brennecke, and T. Esslinger, Dicke quantum phase transition with a superfluid gas in an optical cavity, Nature (London) **464**, 1301 (2010).
[14] J. Klinder, H. Keler, M. Wolke, L. Mathey, and A. Hemmerich, Dynamical phase transition in the open dicke model, Proc. Natl. Acad. Sci. U.S.A. **112**, 3290 (2015).
[15] R. M. Kroeze, Y. Guo, V. D. Vaidya, J. Keeling, and B. L. Lev, Spinor Self-Ordering of a Quantum Gas in a Cavity, Phys. Rev. Lett. **121**, 163601 (2018).
[16] M. Eckstein, M. Kollar, and P. Werner, Thermalization after an Interaction Quench in the Hubbard Model, Phys. Rev. Lett. **103**, 056403 (2009).

[17] M. Schiró and M. Fabrizio, Time-Dependent Mean Field Theory for Quench Dynamics in Correlated Electron Systems, Phys. Rev. Lett. **105**, 076401 (2010).
[18] A. Gambassi and P. Calabrese, Quantum quenches as classical critical films, Europhys. Lett. **95**, 66007 (2011).
[19] P. Smacchia, M. Knap, E. Demler, and A. Silva, Exploring dynamical phase transitions and prethermalization with quantum noise of excitations, Phys. Rev. B **91**, 205136 (2015).
[20] P. Kirton, M. M. Roses, J. Keeling, and E. G. Dalla Torre, Introduction to the dicke model: From equilibrium to nonequilibrium, and vice versa, Adv. Quantum Technol. **2**, 1970043 (2019).
[21] A. F. Volkov and S. M. Kogan, Collisionless relaxation of the energy gap in superconductors, Sov. Phys. JETP **38**, 1018 (1974), http://www.jetp.ac.ru/cgi-bin/e/index/e/38/5/p1018?a=list.
[22] R. A. Barankov, L. S. Levitov, and B. Z. Spivak, Collective Rabi Oscillations and Solitons in a Time-Dependent bcs Pairing Problem, Phys. Rev. Lett. **93**, 160401 (2004).
[23] E. A. Yuzbashyan, V. B. Kuznetsov, and B. L. Altshuler, Integrable dynamics of coupled Fermi-Bose condensates, Phys. Rev. B **72**, 144524 (2005).
[24] E. A. Yuzbashyan, B. L. Altshuler, V. B. Kuznetsov, and V. Z. Enolskii, Nonequilibrium cooper pairing in the nonadiabatic regime, Phys. Rev. B **72**, 220503(R) (2005).
[25] E. A. Yuzbashyan, O. Tsyplyatyev, and B. L. Altshuler, Relaxation and Persistent Oscillations of the Order Parameter in Fermionic Condensates, Phys. Rev. Lett. **96**, 097005 (2006).
[26] R. A. Barankov and L. S. Levitov, Synchronization in the bcs Pairing Dynamics as a Critical Phenomenon, Phys. Rev. Lett. **96**, 230403 (2006).
[27] E. A. Yuzbashyan, M. Dzero, V. Gurarie, and M. S. Foster, Quantum quench phase diagrams of an s-wave bcs-bec condensate, Phys. Rev. A **91**, 033628 (2015).
[28] H. P. Ojeda Collado, J. Lorenzana, G. Usaj, and C. A. Balseiro, Population inversion and dynamical phase transitions in a driven superconductor, Phys. Rev. B **98**, 214519 (2018).
[29] H. P. Ojeda Collado, G. Usaj, J. Lorenzana, and C. A. Balseiro, Fate of dynamical phases of a bcs superconductor beyond the dissipationless regime, Phys. Rev. B **99**, 174509 (2019).
[30] H. P. Ojeda Collado, G. Usaj, J. Lorenzana, and C. A. Balseiro, Nonlinear dynamics of driven superconductors with dissipation, Phys. Rev. B **101**, 054502 (2020).
[31] Y. Pehlivan, A. B. Balantekin, T. Kajino, and T. Yoshida, Invariants of collective neutrino oscillations, Phys. Rev. D **84**, 065008 (2011).
[32] R. Matsunaga, Y. I. Hamada, K. Makise, Y. Uzawa, H. Terai, Z. Wang, and R. Shimano, Higgs Amplitude Mode in the bcs Superconductors $nb_{1-x}ti_xN$ Induced by Terahertz Pulse Excitation, Phys. Rev. Lett. **111**, 057002 (2013).
[33] R. Matsunaga, N. Tsuji, H. Fujita, A. Sugioka, K. Makise, Y. Uzawa, H. Terai, Z. Wang, H. Aoki, and R. Shimano, Light-induced collective pseudospin precession resonating with higgs mode in a superconductor, Science **345**, 1145 (2014).
[34] H. Gao, F. Schlawin, M. Buzzi, A. Cavalleri, and D. Jaksch, Photoinduced Electron Pairing in a Driven Cavity, Phys. Rev. Lett. **125**, 053602 (2020).
[35] M. A. Norcia, R. J. Lewis-Swan, J. R. K. Cline, B. Zhu, A. M. Rey, and J. K. Thompson, Cavity-mediated collective spin-exchange interactions in a strontium superradiant laser, Science **361**, 259 (2018).
[36] E. J. Davis, A. Periwal, E. S. Cooper, G. Bentsen, S. J. Evered, K. Van Kirk, and M. H. Schleier-Smith, Protecting Spin Coherence in a Tunable Heisenberg Model, Phys. Rev. Lett. **125**, 060402 (2020).
[37] V. D. Vaidya, Y. Guo, R. M. Kroeze, K. E. Ballantine, A. J. Kollár, J. Keeling, and B. L. Lev, Tunable-Range, Photon-Mediated Atomic Interactions in Multimode Cavity qed, Phys. Rev. X **8**, 011002 (2018).
[38] H. Ritsch, P. Domokos, F. Brennecke, and T. Esslinger, Cold atoms in cavity-generated dynamical optical potentials, Rev. Mod. Phys. **85**, 553 (2013).
[39] P. Strack and S. Sachdev, Dicke Quantum Spin Glass of Atoms and Photons, Phys. Rev. Lett. **107**, 277202 (2011).
[40] S. Gopalakrishnan, B. L. Lev, and P. M. Goldbart, Frustration and Glassiness in Spin Models with Cavity-Mediated Interactions, Phys. Rev. Lett. **107**, 277201 (2011).
[41] S. P. Kelly, A. M. Rey, and J. Marino, Effect of Active Photons on Dynamical Frustration in Cavity QED, Phys. Rev. Lett. **126**, 133603 (2021)..
[42] E. Colella, S. Ostermann, W. Niedenzu, F. Mivehvar, and H. Ritsch, Antiferromagnetic self-ordering of a fermi gas in a ring cavity, New J. Phys. **21**, 043019 (2019).
[43] V. Gurarie and L. Radzihovsky, Resonantly paired fermionic superfluids, Ann. Phys. (Amsterdam) **322**, 2 (2007).
[44] M. S. Foster, M. Dzero, V. Gurarie, and E. A. Yuzbashyan, Quantum quench in a $p + ip$ superfluid: Winding numbers and topological states far from equilibrium, Phys. Rev. B **88**, 104511 (2013).
[45] E. J. Davis, G. Bentsen, L. Homeier, T. Li, and M. H. Schleier-Smith, Photon-Mediated Spin-Exchange Dynamics of Spin-1 Atoms, Phys. Rev. Lett. **122**, 010405 (2019).
[46] A. Shankar, L. Salvi, M. L. Chiofalo, N. Poli, and M. J. Holland, Squeezed state metrology with bragg interferometers operating in a cavity, Quantum Sci. Technol. **4**, 045010 (2019).
[47] J. M. Radcliffe, Some properties of coherent spin states, J. Phys. A **4**, 313 (1971).
[48] See Supplemental Material, which contains Refs. [9,24, 26,27,35,47,49,50], at http://link.aps.org/supplemental/10.1103/PhysRevLett.126.173601 for a summary of the Lax method used in Figs. 2 and 3 and details of the physical model used in Fig. 4.
[49] M. Foster and V. Gurarie (private communication).
[50] G. R. Dennis, J. J. Hope, and M. T. Johnsson, XMDS2: Fast, scalable simulation of coupled stochastic partial differential equations, Comput. Phys. Commun. **184**, 201 (2013).
[51] R. J. Lewis-Swan, M. A. Norcia, J. R. K. Cline, J. K. Thompson, and A. M. Rey, Robust Spin Squeezing via Photon-Mediated Interactions on an Optical Clock Transition, Phys. Rev. Lett. **121**, 070403 (2018).
[52] It should also be possible to prepare initial states that are split by their projection along the z direction rather than the projection along x (set by $\Delta\phi_0$) that would follow even more closely the BCS ground state. However, varying the relative azimuthal opening angle gives similar

physics and is more robust to typical experimental constraints [48].

[53] C. Lhuillier and F. Laloe, Transport properties in a spin polarized gas, I, J. Phys. France **43**, 197 (1982).

[54] W. J. Gully and W. J. Mullin, Observation of Spin Rotation Effects in Polarized ^{3}He-^{4}He Mixtures, Phys. Rev. Lett. **52**, 1810 (1984).

[55] B. R. Johnson, J. S. Denker, N. Bigelow, L. P. Lévy, J. H. Freed, and D. M. Lee, Observation of Nuclear Spin Waves in Spin-Polarized Atomic Hydrogen Gas, Phys. Rev. Lett. **53**, 302(E) (1984).

[56] E. P. Bashkin, Spin waves and quantum collective phenomena in boltzmann gases, Sov. Phys. Usp. **29**, 238 (1986).

[57] J. M. McGuirk, H. J. Lewandowski, D. M. Harber, T. Nikuni, J. E. Williams, and E. A. Cornell, Spatial Resolution of Spin Waves in an Ultracold Gas, Phys. Rev. Lett. **89**, 090402 (2002).

[58] X. Du, L. Luo, B. Clancy, and J. E. Thomas, Observation of Anomalous Spin Segregation in a Trapped Fermi Gas, Phys. Rev. Lett. **101**, 150401 (2008).

[59] C. Deutsch, F. Ramirez-Martinez, C. Lacroûte, F. Reinhard, T. Schneider, J. N. Fuchs, F. Piéchon, F. Laloë, J. Reichel, and P. Rosenbusch, Spin Self-Rephasing and Very Long Coherence Times in a Trapped Atomic Ensemble, Phys. Rev. Lett. **105**, 020401 (2010).

[60] G. Kleine Büning, J. Will, W. Ertmer, E. Rasel, J. Arlt, C. Klempt, F. Ramirez-Martinez, F. Piéchon, and P. Rosenbusch, Extended Coherence Time on the Clock Transition of Optically Trapped Rubidium, Phys. Rev. Lett. **106**, 240801 (2011).

[61] A. M. Rey, L. Jiang, M. Fleischhauer, E. Demler, and M. D. Lukin, Many-body protected entanglement generation in interacting spin systems, Phys. Rev. A **77**, 052305 (2008).

[62] B. Zhu, J. Schachenmayer, M. Xu, F. Herrera, J. G. Restrepo, M. J. Holland, and A. M. Rey, Synchronization of interacting quantum dipoles, New J. Phys. **17**, 083063 (2015).

[63] K. Y, *Chemical Oscillations, Waves, and Turbulence* (Dover, New York, 2003).

[64] L. F. Santos, F. Borgonovi, and G. L. Celardo, Cooperative Shielding in Many-Body Systems with Long-Range Interaction, Phys. Rev. Lett. **116**, 250402 (2016).

[65] G. L. Celardo, R. Kaiser, and F. Borgonovi, Shielding and localization in the presence of long-range hopping, Phys. Rev. B **94**, 144206 (2016).